

## RESEARCH ARTICLE

# Improving advanced intraoperative MRI methods during pediatric neurosurgery

Pien E. J. Jellema<sup>1,2</sup> | Lilli M. Manssdörfer<sup>1</sup> | Fredy Visser<sup>2,3</sup> |  
 Alberto De Luca<sup>2,4</sup>  | Cynthia L. E. Smit<sup>1</sup> | Eelco W. Hoving<sup>1,5</sup> |  
 Kirsten M. van Baarsen<sup>1,5</sup> | Thomas Lindner<sup>6</sup> | Henk-Jan M. M. Mutsaerts<sup>7,8</sup> |  
 Jan Willem Dankbaar<sup>9</sup> | Maarten H. Lequin<sup>1,9</sup> | Jannie P. Wijnen<sup>2</sup>

<sup>1</sup>Department of Pediatric Neuro-Oncology, Princess Máxima Centre for Pediatric Oncology, Utrecht, The Netherlands

<sup>2</sup>Centre for Image Sciences, University Medical Centre Utrecht, Utrecht, The Netherlands

<sup>3</sup>Philips HealthCare, Best, The Netherlands

<sup>4</sup>Department of Neurology, University Medical Center Utrecht, Utrecht, The Netherlands

<sup>5</sup>Department of Neurosurgery, University Medical Centre Utrecht, Utrecht, The Netherlands

<sup>6</sup>Department of Diagnostic and Interventional Neuroradiology, University Hospital Hamburg-Eppendorf, Hamburg, Germany

<sup>7</sup>Department of Radiology and Nuclear Medicine, Amsterdam UMC Location Vrije Universiteit Amsterdam, Amsterdam, The Netherlands

<sup>8</sup>Amsterdam Neuroscience, Brain Imaging, Amsterdam, The Netherlands

<sup>9</sup>Department of Radiology, University Medical Centre Utrecht, Utrecht, The Netherlands

## Correspondence

Pien E. J. Jellema, Department of Pediatric Neuro-Oncology, Princess Máxima Centre for Pediatric Oncology, Utrecht, The Netherlands. Email: [e.j.jellema@prinsesmaximacentrum.nl](mailto:e.j.jellema@prinsesmaximacentrum.nl)

## Funding information

We gratefully acknowledge funding of the European Union: Eurostars E! 12449 IMAGINE! and the Dutch Research Council: NWO-VIDI 18361\_JW.

## Abstract

Advanced intraoperative MR images (ioMRI) acquired during the resection of pediatric brain tumors could offer additional physiological information to preserve healthy tissue. With this work, we aimed to develop a protocol for ioMRI with increased sensitivity for arterial spin labeling (ASL) and diffusion MRI (dMRI), optimized for patient positioning regularly used in the pediatric neurosurgery setting. For ethical reasons, ASL images were acquired in healthy adult subjects that were imaged in the prone and supine position. After this, the ASL cerebral blood flow (CBF) was quantified and compared between both positions. To evaluate the impact of the RF coils setups on image quality, we compared different setups (two vs. four RF coils) by looking at T1-weighted (T1w) signal-to-noise ratio (SNR) and contrast-to-noise ratio (CNR), as well as undertaking a qualitative evaluation of T1w, T2w, ASL, and dMR images. Mean ASL CBF did not differ between the surgical prone and supine positions in any of the investigated regions of interest or the whole brain. T1w SNR (gray matter:  $p = 0.016$ , 34% increase; white matter:  $p = 0.016$ , 32% increase) and CNR were higher ( $p = 0.016$ ) in the four versus two RF coils setups ( $18.0 \pm 1.8$  vs.  $13.9 \pm 1.8$ ). Qualitative evaluation of T1w, T2w, ASL, and dMR images resulted in acceptable to good image quality and did not differ statistically significantly between setups. Only the nonweighted diffusion image maps and corticospinal tract reconstructions yielded higher image quality and reduced susceptibility artifacts with four RF coils. Advanced ioMRI metrics were more precise with four RF coils as the standard deviation decreased. Taken together, we have investigated the practical use of advanced ioMRI during pediatric neurosurgery. We conclude that ASL CBF quantification in the surgical prone position is valid and that ASL and dMRI acquisition with two RF coils can be performed adequately for clinical use. With four versus two RF coils, the SNR of the images increases, and the sensitivity to artifacts reduces.

**Abbreviations:** ASL CBF, arterial spin labeling cerebral blood flow; CNR, contrast-to-noise ratio; dMRI, diffusion MRI; GM, gray matter; ioMRI, intraoperative MRI; SNR, signal-to-noise ratio; WM, white matter.

This is an open access article under the terms of the [Creative Commons Attribution](https://creativecommons.org/licenses/by/4.0/) License, which permits use, distribution and reproduction in any medium, provided the original work is properly cited.

© 2024 The Authors. *NMR in Biomedicine* published by John Wiley & Sons Ltd.

## KEYWORDS

arterial spin labeling, diffusion MRI, intraoperative, neurosurgery, pediatrics

## 1 | INTRODUCTION

Intraoperative MRI (ioMRI) in pediatric brain tumor surgery aims to increase resection control. As ioMRI accounts for the brain shift that results from the craniotomy, it provides a more accurate update to the neuronavigation.<sup>1</sup> Conventionally, ioMRI protocols based on anatomical T1- and T2-weighted (T1w and T2w, respectively) MR images are needed to assess the extent of resection.<sup>2</sup> Nevertheless, advanced MR sequences are said to offer additional physiological information during surgery, aiding in the preservation of healthy and functional brain regions.<sup>3-5</sup> For example, arterial spin labeling (ASL) can provide information on intraoperative cerebral blood flow (CBF).<sup>6</sup> An intraoperative update of fiber tractography, based on diffusion MRI (dMRI), could help to prevent surgery-associated neurological damage in surrounding brain tissue.<sup>7-9</sup> Moreover, intraoperative dMRI can also detect ischemic infarcts.<sup>10</sup>

The available literature on advanced ioMRI sequences in pediatric populations is limited,<sup>11</sup> which can probably be attributed to the challenges of performing experimental imaging studies with limited available time during surgery. The acquisition of advanced MR images is also challenged by patients operated in the prone position because of the high prevalence of tumors in the posterior fossa region in the pediatric population.<sup>12,13</sup> Another challenge of advanced ioMRI acquisition is that only two single-channel flexible receive coils (RF coils) can be combined with the DORO surgical head fixation frame and the Philips MR system.<sup>6</sup> Using only two RF coils could compromise the image quality of the advanced sequences due to limited options for parallel imaging.

The acquisition of MR images in the prone position could pose a challenge for the ASL sequence because the arteries labeled in ASL sequences are in a different orientation and rotation in the prone position, where patients lie on their belly with their heads tilted downward. Suboptimal labeling efficiency of these arteries can result in inaccurate ASL CBF quantification.<sup>14</sup> It is unknown whether quantified ASL CBF differs within patients in the surgical prone or supine position.

The image quality challenge in advanced ioMRI acquisition with two RF coils arises from the limited scanning time during surgery, the relatively low signal-to-noise ratio (SNR) of advanced sequences,<sup>4,5,15</sup> and the restricted applicability of acceleration techniques, such as parallel imaging (e.g., SENSE) or Compressed Sensing, with a limited number of RF coils. Additional RF coils could impact image quality as they theoretically increase the geometry ( $g$ ) factor and, consequently, SENSE's undersampling capabilities.<sup>16</sup> Ultimately, this should result in fewer susceptibility artifacts, which could be translated into improved image quality. Alternatively, sequences that use Compressed Sensing denoised reconstructions could improve theoretically with more signal from more RF coils.<sup>17</sup> While other ioMRI systems with multiple RF coils are available, such as MR systems from other vendors or the NORAS head-frame with eight integrated receive channels,<sup>3</sup> our institution favors the use of the DORO frame. This preference is attributed to the high surgical flexibility, particularly in the pediatric population, which exhibits a wide range of tumor locations. Therefore, there is a need for flexibility in head positioning to secure optimal surgical entry in the brain.

With this work, we aimed to explore the validity of ASL and dMRI acquisition during pediatric neurosurgery with a focus on patient positioning and RF coils setup. To this end, we first investigated if ASL CBF differs between the surgical prone and supine positions in the standard clinical setup (32-channel head coil). Second, we developed an ioMRI setup that can provide high-quality ASL and multishell dMRI, as well as T1w and T2w images, with four RF coils that still allowed optimal head positioning in the head-frame for neurosurgery. The original protocol for the two RF coils was derived from our institution's standard clinical pediatric brain tumor protocol. The protocol for the four RF coils has been optimized for SENSE (ASL and dMRI) and Compressed Sensing reconstructions (T1w and T2w), while maintaining similar acquisition times and spatial resolutions as for the two RF coils setup. The validation of prone ASL CBF was measured with quantified ASL CBF and the optimal ASL labeling efficiency with flow velocity.<sup>14</sup> Differences in image quality obtained with the two and four RF coils were measured for SNR, contrast-to-noise ratio (CNR), and qualitative image analysis. Because of ethical considerations when scanning children, healthy adults were included as our study population.

## 2 | EXPERIMENTAL

### 2.1 | Study population

For the first part of our study (ASL in the prone position), five healthy subjects (aged 22–31 years; three females) were included. Another seven healthy subjects (aged 21–29 years; four females) were included for the second part (multiple RF coils). The local ethics committee approved this study. All subjects provided written informed consent.

## 2.2 | Part 1: ASL in the prone position

### 2.2.1 | Experimental setup

To validate the ASL CBF measurements in the prone position, subjects were scanned in the standard clinical setup on a 3-T MRI scanner (Ingenia Elition X, version 5.7.1.2, Philips Healthcare, Best, The Netherlands) with the 32-channel head coil. Subjects were scanned in the prone and supine position during the same MRI examination. To mimic the surgical prone position, subjects lay on their belly with their chest lifted with MRI-compatible table pads so their head could tilt downward. In the supine position, the subjects would lie on their back with their head in a neutral position. Foam padding was used to restrict head motion and cushioning in both positions. ASL CBF data quality was also verified in the prone position in the ioMRI setup with the two RF coils (see the [supporting information](#)).

### 2.2.2 | Imaging protocol

The imaging protocol (Table 1) consisted of a T1w imaging acquisition and a standard 3D phase contrast (PC) angiography survey with a large volume that imaged all the carotid arteries. The maximum intensity projection reconstruction of this survey scan was used for planning purposes of the standard pulse-wave triggered 2D quantitative PC MRI and the pseudocontinuous ASL (PCASL) image acquisition. The T1w and PCASL acquisition parameters were derived from the clinical pediatric brain tumor protocols established at our institution. Note that this imaging protocol was scanned with the 32-channel head coil but optimized in such a way that the same protocol can also be used with two RF coils. Therefore, no SENSE has been used.

### 2.2.3 | Image postprocessing

ASL CBF images were quantified with the ExploreASL ([ExploreASL.com](#)) pipeline. This toolbox is based on MATLAB (MathWorks, Natick, MA, USA), Statistical Parametric Mapping (SPM), and Diffeomorphic Anatomical Registration analysis using Exponentiated Lie algebra (DARTTEL).<sup>18</sup> Within the ExploreASL pipeline, the Computational Anatomy Toolbox 12 (CAT12) was used for the segmentation of T1w images into partial volume gray matter (GM), partial volume white matter (WM), and cerebrospinal fluid with the Montreal Neurological Institute (MNI) template. Furthermore, motion correction and outlier removal were executed in the control and labeled images. The remaining images were registered to the partial volume GM map of the T1w image. CBF quantification was performed assuming the one-compartment model.<sup>19</sup>

**TABLE 1** Imaging parameters of all sequences used to study ASL in the prone position.

Sequence	T1w	Quantitative PC MRI	PCASL
General parameters			
Field of view (mm)	230 × 230 × 190	150 × 100	238 × 238 × 161
Acquired voxel size (mm)	1.00 × 1.00 × 1.00	1.15 × 1.15 × 5.00	2.98 × 2.98 × 7.00
Echo time (ms)	3.83	5.66	12.10
Repetition time (ms)	8.32	9.29	4100
Flip angle (°)	8	10	90
Acquisition time	3 min 14 s	1 min 53 s	4 min 47 s
Number of slices	190	1	23
Sequence specific parameters			
Shot interval (ms)	3000		
Time inversion (ms)	900		
Velocity encoding (cm/s)		90	
Dynamic volumes			8
Postlabeling delay (ms)			1500
Labeling duration (ms)			1800
Label distance (mm)			109.86

Note: The quantitative PC MRI had a 2D readout and the PCASL sequence had a 3D GraSE readout. No acceleration was used. Abbreviations: ASL, arterial spin labeling; PC, phase contrast; PCASL, pseudocontinuous arterial spin labeling; T1w, T1-weighted.

Mean ASL CBF values were obtained for the whole brain and several regions of interest (ROIs), including the cerebellum, frontal, temporal, parietal, and occipital lobes. The automated ROI segmentation of ExploreASL was based on the MNI Structural atlas and the Wholebrain atlas. Partial volume correction was only applied to the CBF quantification of the ROIs, not to the whole-brain measurements.

The 2D quantitative PC MRI data were processed using Philips Qflow MRI software. After manually placing ROIs in the left and right internal carotid artery and vertebral artery, mean arterial flow velocity values were obtained from each artery.

## 2.2.4 | Statistical analysis

To analyze differences in quantified ASL CBF values and flow velocity between the prone and supine positions within subjects, the paired Wilcoxon signed-rank test (significance level  $p < 0.05$ ) was used for each ROI separately.

## 2.3 | Part 2: Multiple RF coils

### 2.3.1 | Experimental setup

For each subject, images with both the two and four RF coils setups were obtained during the same MRI examination on a 3-T MRI scanner (Ingenia, 70-cm bore, version 5.7.1.3, Philips Healthcare) (Figure 1). In the two RF coils setup, two Philips FLEX L coils (20-cm diameter) were connected to a Philips dStream interface box. For the four RF coils scenario, another dStream interface box was stacked on top of the first one, which allowed the connection of two additional FLEX M coils (15-cm diameter). The two dStream interface boxes were used to mimic an interface box with four sockets for the FLEX coils that is not yet commercially available. For the four RF coils setup, the optimal positioning was determined of two overlapping RF coils with respect to each other by minimizing the S12 (i.e., the parameter that describes the amount of coupling) using two pickup probes, each at a fixed distance per RF coil, connected to a network analyzer. The optimal decoupling was achieved when the neighboring RF coils were approximately 3 cm at 30° in overlap (Figure 1). In both setups, the subject was positioned in the supine position, as described in part 1.

### 2.3.2 | Imaging protocol

The scan protocol consisted of T1w, T2w, ASL, and dMRI acquisitions. The two RF coils protocol was derived from the preoperative protocol of our institution that is normally acquired with a 32-channel head coil. For our study, we optimized the SENSE factors for the acquisition with two RF coils and a total duration of ~20 min. The protocol with four RF coils had the same acquisition time and resolution but was optimized for image quality using SENSE or Compressed Sensing (Table 2). The T1w image acquisition had a second identical scan with the radiofrequency transmitter and gradient amplifiers switched off to produce a modulus noise scan needed to calculate SNR. The T1w and T2w acquisition parameters were optimized for Compressed Sensing (factor 1.8) with different denoise factors (see the qualitative analysis part in the [supporting information](#)). The PCASL acquisition parameters differed primarily in their SENSE factors and dynamic volumes (two RF coils: SENSE 1, dynamic volumes 8; four RF coils: SENSE 2, dynamic volumes 16), and the multishell dMRI acquisitions differed in their SENSE factors to reduce susceptibility artifacts (two RF coils: SENSE 1.8; four RF coils: SENSE 2.5). For the PCASL and -dMRI protocols with two RF coils, the TEs and TRs were first set to “shortest” and then fixed. To keep similar image contrast and acquisition times in both protocols, the same TE and TR values of the two RF coils protocol were used for the acquisition with four RF coils.

### 2.3.3 | Image postprocessing

The SNR and CNR were calculated based on the T1w images. After brain extraction (BET FSL toolbox), signal maps were registered to MNI space (FLIRT FSL toolbox) and segmented into GM and WM using FAST FSL toolbox.<sup>20</sup> The images without RF excitations (reconstructed using the identical complex weighting factors as used for the MRI reconstructions) were translated into a noise map using a standard deviation kernel of  $9 \times 9 \times 9$  voxels.<sup>21</sup> The GM and WM segments were used to delineate the corresponding noise voxels in the noise image.

CBF quantification of the PCASL data was processed as described with the ExploreASL pipeline. Left and right GM were included as ROIs for the ASL CBF quantification. Both were corrected for partial volume effects. To calculate the SNR of the ASL CBF maps, whole-brain T1w GM segments were used to delineate the corresponding voxels of the SNR maps. Both the T1w GM segments and the SNR maps were derived from the

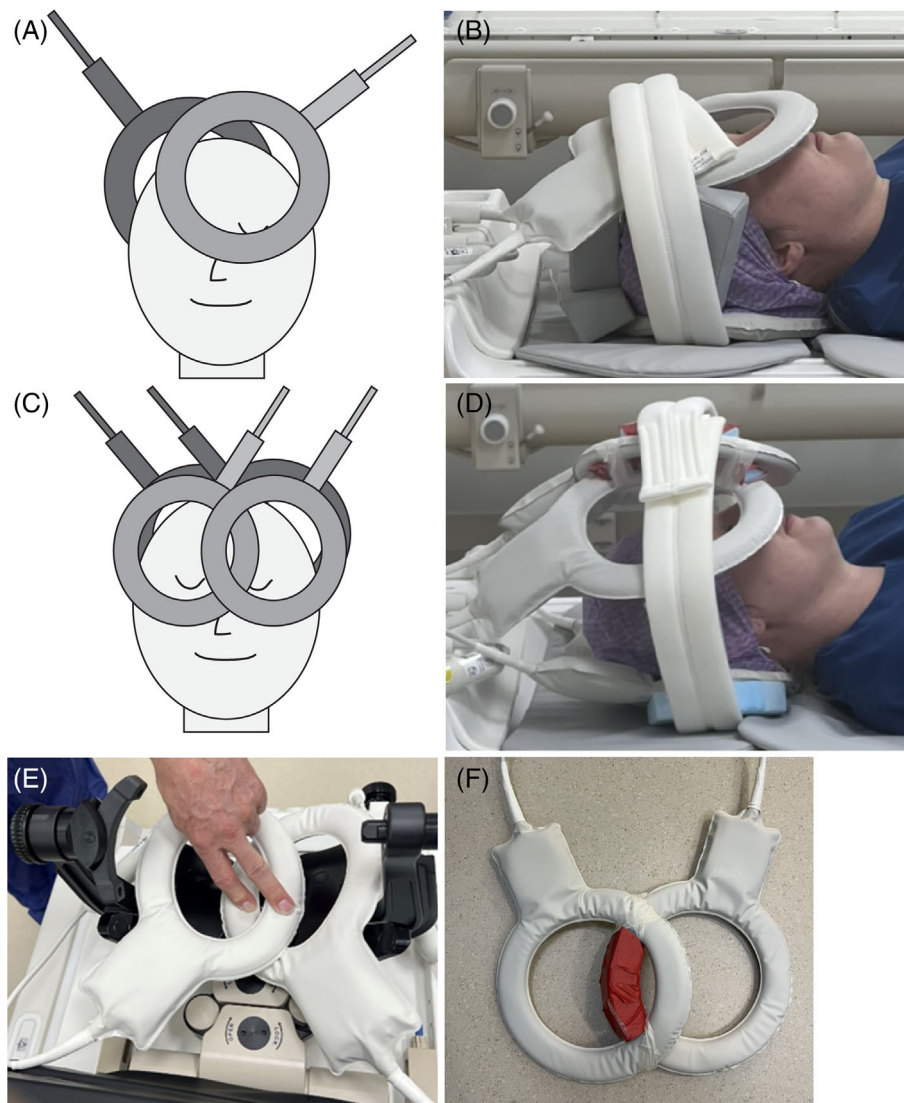


**FIGURE 1** Experimental setup of two and four RF coils used for intraoperative MRI acquisition. (A) Illustration of the setup with two standard Philips FLEX L coils (20-cm diameter). (B) Side view of the setup with two RF coils. The coils were fixated with a fabric strap and supported with foam cushions. (C) Illustration of the setup with four RF coils in overlap position: anterior two standard Philips FLEX M coils (15-cm diameter) and posterior two standard Philips FLEX L coils (20-cm diameter). (D) Side view of the setup with four RF coils. (E) The anterior FLEX M coils fit in overlap position in the DORO surgical head-frame. These elements were fixated with tape before scanning. (F) The posterior FLEX L coils were fixated with a piece of foam (red) and tape to maintain the optimal spatial overlap for maximum decoupling.

Explore ASL population module. Explore ASL generates voxel-wise SNR maps by dividing the mean ASL CBF by the standard deviation across the control-label repetitions.<sup>19</sup> This was done for each subject and setup.

The multishell dMRI data were used to reconstruct quantitative maps of WM microstructure and to perform fiber tractography of eloquent pathways such as the corticospinal tract (CST) and the arcuate fasciculus (AF). To achieve this, the multishell dMRI data were preprocessed with a fully automated pipeline based on MRIToolkit (<https://github.com/delucaal/MRIToolkit.git>) and ExploreDTI.<sup>22,23</sup> Data preprocessing included correction for signal drift,<sup>24</sup> denoising with the MPPCA method, brain masking, correction for eddy currents and subject motion by means of affine registration, b-matrix correction,<sup>25</sup> and EPI distortions correction by means of a nonlinear b-spline registration to the T1w image. After preprocessing, the diffusion kurtosis imaging model was fit to the data using the mean kurtosis (MK) curve correction method,<sup>26,27</sup> then maps of fractional anisotropy (FA), mean diffusivity (MD), and MK were derived as in our previous study.<sup>28</sup> To reconstruct fiber tracts, the Generalized Richardson Lucy spherical deconvolution method<sup>22</sup> was applied to reconstruct fiber orientation distributions in WM while accounting for partial volume with GM and cerebrospinal fluid, then deterministic fiber tractography was performed. Whole-brain tractography was performed by seeding all voxels within the brain mask, with the parameters step-size 1 mm and 45° angle threshold. Finally, the CST and AF were segmented from the whole-brain tractography by applying the WM analysis pipeline,<sup>29</sup> and their mean FA, MD, and MK were calculated. For the calculation

TABLE 2 Imaging parameters of all sequences measured with two and four RF coils.

Sequence	T1w		T2w		PCASL		dMRI (multishell)	
	2	4	2	4	2	4	2	4
General parameters								
Field of view (mm)	351 × 351 × 160	351 × 351 × 160	230 × 179 × 154	230 × 179 × 154	240 × 240 × 160	240 × 240 × 160	240 × 240 × 150	240 × 240 × 150
Acquired voxel size (mm)	1.2 × 1.2 × 1.2	1.2 × 1.2 × 1.2	0.8 × 0.9 × 4	0.8 × 0.9 × 4	3.75 × 3.75 × 7	3.75 × 3.75 × 7	2.5 × 2.5 × 2.5	2.5 × 2.5 × 2.5
Echo time (ms)	2.1	2.1	110	110	11.5	11.5	99	99
Repetition time (ms)	4.7	4.7	3734	3734	4100	4100	7900	7900
Flip angle (°)	10	10	90	90	90	90	90	90
Acceleration	1.8 <sup>a</sup>	1.8 <sup>a</sup>	1 <sup>a</sup>	1 <sup>a</sup>	1 <sup>b</sup>	2 <sup>b</sup>	1.8 <sup>b</sup>	2.5 <sup>b</sup>
Acquisition time	3 min 52 s	3 min 52 s	3 min 55 s	3 min 55 s	4 min 32 s	4 min 32 s	7 min 57 s	7 min 57 s
Number of slices	133	133	39	39	23	23	60	60
Sequence specific parameters								
Shot interval (ms)	3000	3000						
Time inversion (ms)	900	900						
Dynamic volumes	2	2			8	16		
Postlabeling delay (ms)					1500	1500		
Labeling duration (ms)					1800	1800		
Label distance (mm)					109.86	109.86		
B-values (s/mm <sup>2</sup> )							0, 1000, 2000	0, 1000, 2000

Note: Note that Compressed Sensing cannot be used in EPI sequences such as often used for ASL and dMRI. The PCASL sequence had a 3D GraSE readout. Multishell dMRI included 6 b0, 20 b1000, and 32 b2000 volumes.

Abbreviations: ASL, arterial spin labeling; dMRI, diffusion MRI; PCASL, pseudocontinuous arterial spin labeling; T1w, T1-weighted; T2w, T2-weighted.

<sup>a</sup>Compressed Sensing factor.

<sup>b</sup>SENSE factor.

of the SNR maps, the mean of all nonweighted diffusion volumes ( $b = 0 \text{ s/mm}^2$ ) was divided by the standard deviation of these volumes. The T1w WM segments were used to delineate the corresponding SNR voxels for each subject and setup.

### 2.3.4 | Quantitative analysis

The SNR and CNR were calculated based on the T1w signal map and the aforementioned modulus noise scan that was used to estimate the noise. SNR was voxel-wise calculated as the T1w signal divided by the noise within the GM and WM segments separately. CNR was calculated as the absolute difference between the mean signal in the GM and WM segments, divided by the mean sum of GM and WM noise.

### 2.3.5 | Qualitative analysis

Two neuroradiologists, with 7.5 and 25 years of experience, rated the MR images. They were blinded to the number of RF coils and the subject identification.

Additionally, the order of the images was reversed between raters to partially counterbalance potential practice and fatigue effects. A monitor resolution of  $1920 \times 1080$  pixels was used for the display and evaluation of the MR images. T1w and T2w images were rated in FSLeyes (version 6.0). Qualitative PCASL perfusion, a nonweighted diffusion image ( $b = 0 \text{ s/mm}^2$ ) map, and FA maps were inspected using Multi-image Analysis GUI (Mango version 4.1; <http://ric.uthscsa.edu>). The neuroradiologists conducted their rating over four separate sessions on different days, further mitigating potential fatigue effects.

Assessment of T1w and T2w images included overall image quality, anatomical details (cortical, subcortical, cerebellum, and gray-white matter contrast), rated on a five-point Likert scale from 1 (very poor) to 5 (excellent).<sup>30</sup>

Qualitative ASL perfusion and nonweighted diffusion image maps were evaluated using an adapted version of a standardized scoring system.<sup>31</sup> This system considered the visibility of components in different brain regions, including the cortex, subcortex, and cerebellum, and the differentiation between GM and WM. The system also considered the presence of artifacts, such as signal drop, distortion, and bright spots or areas.

FA color-coded maps and fiber tractography of the CST, and AF, were evaluated based on the complete representation of anatomy on a five-point Likert scale from 1 (very poor) to 5 (excellent). False positives were rated on a scale from 1 (severe) to 5 (none). The CST and AF were selected based on their representativity for the dorsal-caudate and inferior–superior axis, respectively.

### 2.3.6 | Statistical analysis

To analyze differences in T1w SNR and CNR, dMRI FA and MD, quantified ASL CBF values, and qualitative image scores, the paired Wilcoxon signed-rank test was used (significance level  $p < 0.05$ ). A Cohen's  $\kappa$  was calculated to assess the interobserver agreement between the neuroradiologists for the qualitative image analysis scores for both the setups with two and four RF coils.

## 3 | RESULTS

### 3.1 | Part 1: Quantified ASL CBF in the prone position

Mean whole-brain ASL CBF values, not corrected for partial volume effects, did not show any statistically significant differences between the prone and supine position (prone:  $30.5 \pm 6.75$ , supine:  $33.9 \pm 6.84$  CBF mL/100 g/min). This is also illustrated in Figure 2, which shows the quantified ASL CBF maps of one subject. Similar to the mean population values, no clear difference between positions could be detected in the data of this particular subject. The ASL CBF measurements in each ROI, corrected for partial volume effects, did not differ statistically significantly ( $p > 0.05$ ) between the positions (Figure 3). Some ROIs showed a slightly lower ASL CBF in the prone position compared with the supine position. This was seen in the frontal lobes (prone:  $65.3 \pm 13.0$ , supine:  $69.5 \pm 11.6$  CBF mL/100 g/min,  $p = 0.19$ ) and parietal lobes (prone:  $65.5 \pm 13.6$ , supine:  $69.2 \pm 11.8$  CBF mL/100 g/min,  $p = 0.19$ ). In some ROIs this trend was somewhat stronger, such as in the cerebellum (prone:  $36.1 \pm 9.23$ , supine:  $42.5 \pm 8.09$  CBF mL/100 g/min,  $p = 0.06$ ), occipital (prone:  $52.1 \pm 13.3$ , supine:  $56.3 \pm 10.4$  CBF mL/100 g/min,  $p = 0.06$ ), and temporal lobes (prone:  $43.6 \pm 10.0$ , supine:  $48.7 \pm 9.01$  CBF mL/100 g/min,  $p = 0.06$ ). These results did not differ between genders and did not correlate with age. Therefore, neither gender nor age was included in the statistical analysis as a covariate.

The flow velocity results are described in the [supporting information](#).

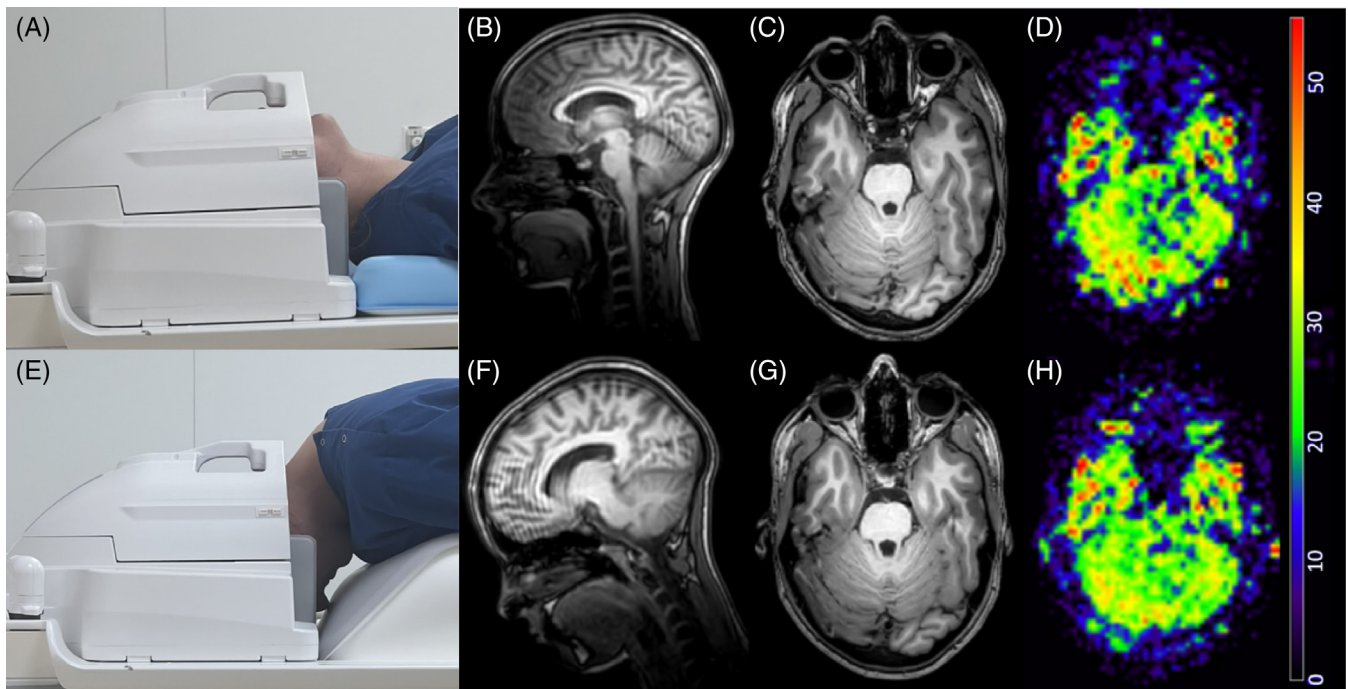


**FIGURE 2** Similar quantified arterial spin labeling (ASL) cerebral blood flow (CBF) results for the same subject in the supine and prone positions. (A) Supine subject positioning in 32-channel head coil. (B) Sagittal T1-weighted (T1w) image. (C) Transverse T1w image. (D) Quantified ASL CBF map (in mL/min/100 g). (E) Prone subject positioning in 32-channel head coil. (F) Sagittal T1w image. (G) Transverse T1w image. (H) Quantified ASL CBF map (in mL/min/100 g).

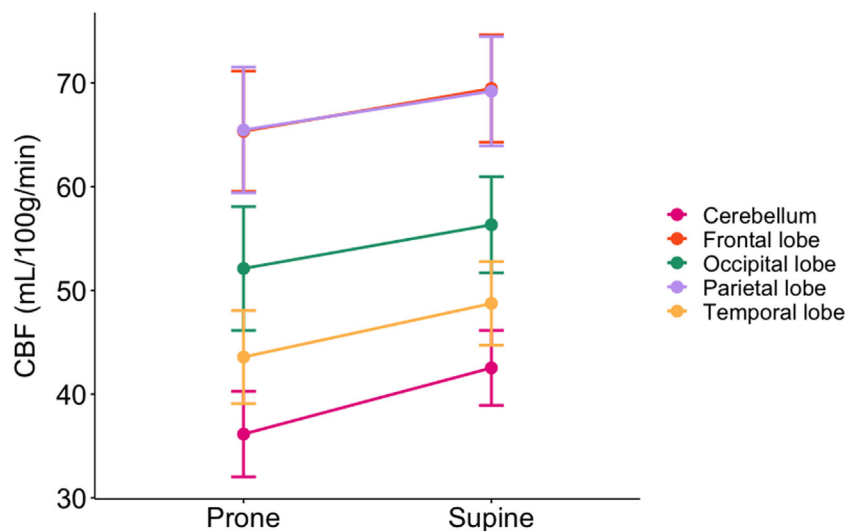


**FIGURE 3** Arterial spin labeling (ASL) cerebral blood flow (CBF) measurements in the supine and prone positions. Mean CBF values (mL/100 g/min) results are shown with error bars in regions of interest (ROIs). No statistically significant differences ( $p > 0.05$ ) were found in any ROI between both positions.

## 3.2 | Part 2: Image quality with multiple RF coils

### 3.2.1 | Quantitative analysis

Mean T1w SNR was statistically significantly higher in the setup with four RF coils than in the one with two RF coils in both GM ( $p = 0.016$ ) and WM ( $p = 0.016$ ) segments, as seen in Figure 4A. For GM and WM, the mean SNR increased by 42% in the four RF coils setup compared with the setup with two RF coils. Interestingly, SNR measured per voxel showed more variation in the four RF coils setup, compared with the one with

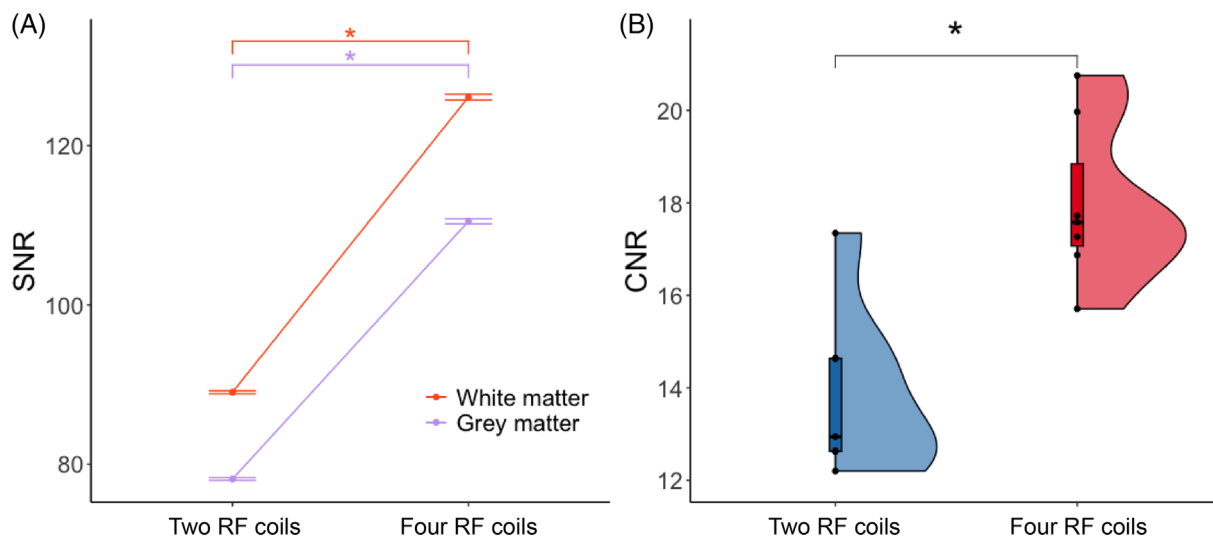


**FIGURE 4** Difference in signal-to-noise ratios (SNRs) and contrast-to-noise ratios (CNRs). (A) Mean SNRs and error bars are shown in gray and white matter for the two and four RF coils setups. (B) Violin plots of the CNR distribution across subjects measured with the two and four RF coils setups. \* $p < 0.05$ .

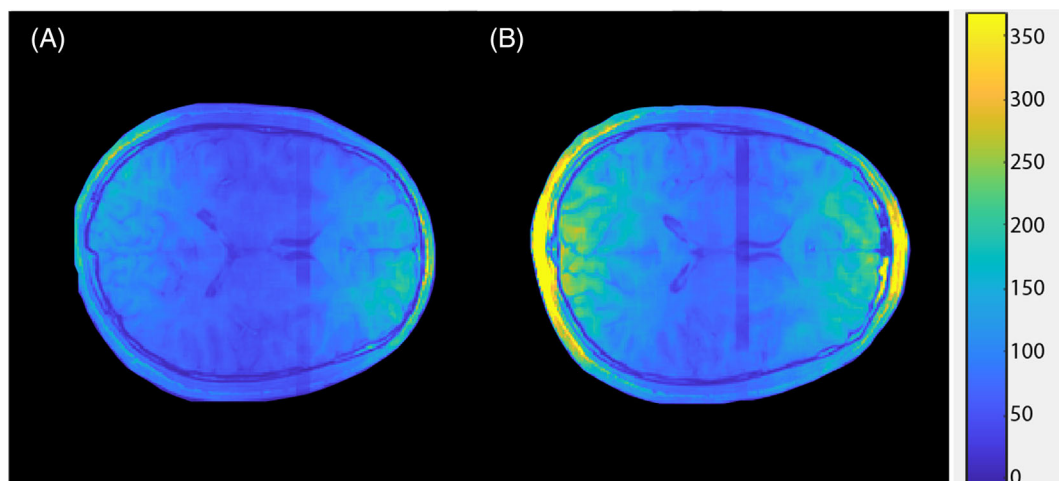


**FIGURE 5** T1-weighted signal-to-noise ratio (SNR) maps with an artifact that originates from the noise reconstruction. The SNR (in arbitrary units) is indicated with the color bar. The SNR distribution of the two RF coils setup (A) is more homogeneous across the whole brain. SNR is increased in the regions closer to the coils and is decreased in deeper seated regions. This effect is increased in the four RF coils setup (B). (B) shows a more widespread range of SNR distribution; however, the SNR in the center of the brain is similar or higher compared with (A).

two RF coils, as the standard deviations in both segments increased strongly (GM: 81%, WM: 100%). This was also seen in the SNR distribution of both setups in the example of one subject (Figure 5). This figure shows a more homogeneously SNR distribution across the whole brain for the data with two RF coils and a more heterogeneous distribution of the four RF coils data. In particular, the areas near the skull showed a stronger increase in SNR for the four RF coils setup. The mean CNR was also statistically higher ( $p = 0.016$ ) for the four RF coils data ( $18.0 \pm 1.8$ ) compared with the two RF coils data ( $13.9 \pm 1.8$ ) (Figure 4B). None of the SNR or CNR results were corrected for gender or age, as they did not correlate with the results.

### 3.2.2 | Qualitative analysis

Mean scores across all imaging sequences indicate that images acquired in the four RF coils setup consistently had superior image quality and similar artifacts compared with the images acquired in the two RF coils setup, although this difference was only marginal. Across all sequences and items, the mean scores ranged from 3 (acceptable) to 5 (excellent). The difference in mean scores ranged from 0 to 0.7 points (Table 3). Figure 6 shows examples of all images that were acquired in one subject with four RF coils for the qualitative analysis.

**TABLE 3** Mean image scores of both neuroradiologists for all sequences measured with two and four RF coils.

	Item	Two coils Mean (sd)	Four coils Mean (sd)	p value
T1w	Overall image quality	4.1 (0.5)	4.2 (0.6)	0.78
	Anatomical details			
	Cortical	4.3 (0.6)	4.4 (0.5)	0.57
	Subcortical	4.3 (0.6)	4.4 (0.5)	0.77
	Cerebellum	3.9 (0.6)	4.1 (0.6)	0.66
	Gray-white matter contrast	4 (0.4)	4.1 (0.3)	0.77
	Artifacts			
	Susceptibility	4.8 (0.4)	4.9 (0.3)	1
	Other	5 (0)	5 (0)	NA
T2w	Overall image quality	4 (0.3)	4 (0.3)	1.00
	Anatomical details			
	Cortical	3.9 (0.3)	4 (0)	1.00
	Subcortical	3.9 (0.3)	4 (0)	1.00
	Cerebellum	4 (0.4)	4 (0)	1.00
	Gray-white matter contrast	3.9 (0.5)	3.8 (0.4)	0.4
	Artifacts			
	Other	5 (0)	5 (0)	NA
ASL	Contrast component			
	Cortical	3.7 (0.5)	3.9 (0.4)	0.48
	Subcortical	3.4 (0.8)	3.8 (0.4)	0.17
	Cerebellum	3.4 (0.6)	3.2 (1)	0.52
	Gray-white matter contrast	3.8 (0.4)	3.9 (0.3)	0.42
	Artifacts			
	Signal drop	4.5 (0.5)	4.4 (0.8)	0.80
	Bright spots and areas	4.5 (0.5)	4.6 (0.6)	0.77
Distortion	4.2 (0.7)	4.4 (0.9)	0.52	
Nonweighted diffusion image	Overall image quality	3.2 (0.6)	3.3 (0.6)	0.78
	Contrast component			
	Cortical	3.1 (0.4)	3.4 (0.6)	0.23
	Subcortical	3 (0.4)	3.5 (0.5)	<b>0.01</b>
	Cerebellum	3 (0.6)	3.6 (0.5)	<b>0.03</b>
	Artifact			
	Susceptibility	3.5 (0.4)	3.9 (0.6)	0.82
Distortion	3.8 (0.7)	3.9 (0.5)	0.07	
FA-map	Completeness of representation	3.5 (0.5)	3.6 (0.5)	0.77
	Artifact			
False positives	3 (0.8)	3.1 (0.8)	0.52	
AF	Completeness of representation	3 (0.7)	3.1 (0.8)	0.57
	Artifact			
False positives	3.2 (0.9)	3.3 (0.9)	0.83	
CST	Completeness of representation	3.1 (0.8)	3.8 (0.5)	<b>0.04</b>
	Artifact			
False positives	3.3 (0.8)	3.5 (0.9)	0.77	

Note: p values in bold indicate a significant result ( $p < 0.05$ ). The Wilcoxon signed-rank test would result in NA if there is no variability between the compared data points.

Abbreviations: AF, arcuate fasciculus; ASL, arterial spin labeling; CST, corticospinal tract; FA, fractional anisotropy; T1w, T1-weighted; T2w, T2-weighted.

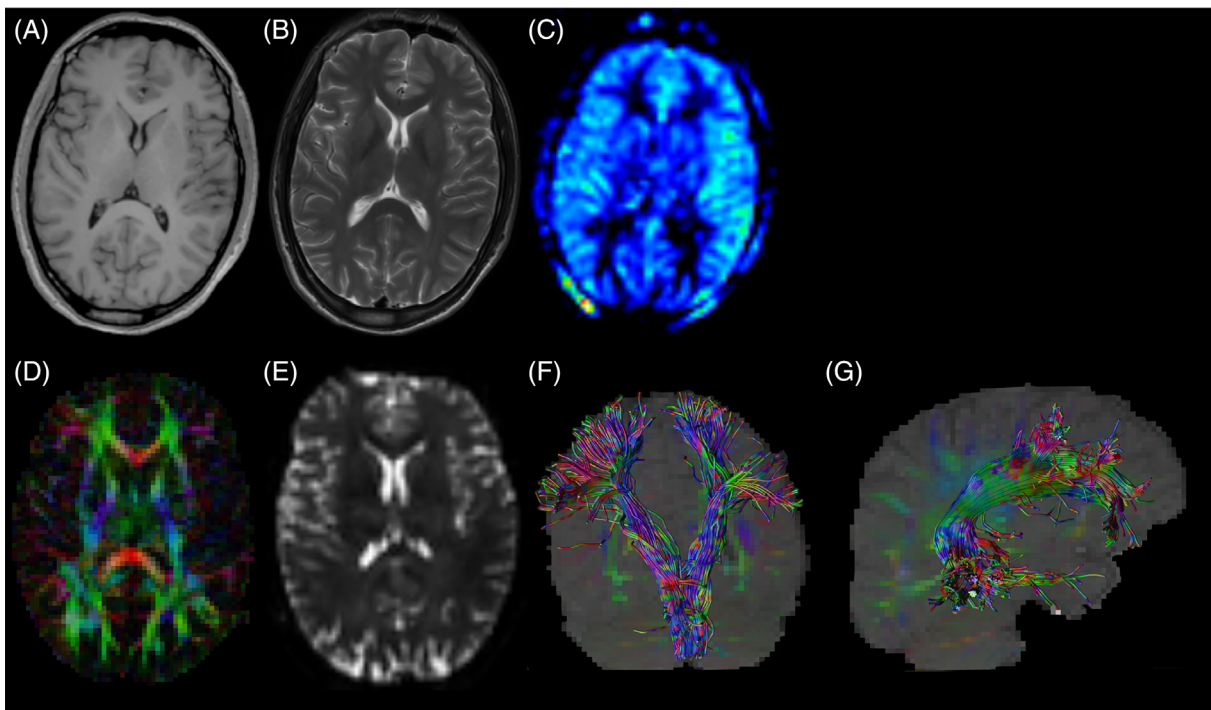


**FIGURE 6** Example axial slices of the images measured with four RF coils in one subject. (A) T1-weighted image. (B) T2-weighted image. (C) Qualitative arterial spin labeling (ASL) perfusion map. (D) Diffusion MRI fractional anisotropy (FA) weighted color-coded map. (E) Nonweighted diffusion image ( $b = 0 \text{ s/mm}^2$ ) map. (F) Reconstruction of corticospinal tract. (G) Reconstruction of arcuate fasciculus.

The most pronounced advantage of the setup with four RF coils, compared with the one with two, for imaging was evident in the nonweighted diffusion image map of the cerebellum (two RF coils mean =  $3.0 \pm 0.55$ , four RF coils mean =  $3.57 \pm 0.51$ ,  $p = 0.03$ ), subcortical volumes (two RF coils mean =  $3.0 \pm 0.39$ , four RF coils mean =  $3.5 \pm 0.52$ ,  $p = 0.01$ ). Further, reconstructions of the CST were evaluated as more complete based on images acquired with four RF coils compared with the two RF coils setup (two RF coils mean =  $3.07 \pm 0.83$ , four RF coils mean =  $3.64 \pm 0.5$ ,  $p = 0.04$ ).

Both neuroradiologists indicated that nonweighted diffusion images acquired in the two RF coils setup were rated lower because they appeared “blurry” compared with the images acquired in the four RF coils setup, which were rated higher. Susceptibility artifacts were also rated lower in the nonweighted diffusion images acquired in the four RF coils (two RF coils mean =  $3.50 \pm 0.65$ ; four RF coils mean  $3.95 \pm 0.48$ ).

Interobserver agreement for all sequences was fair for both the images acquired with the two and four RF coils, with Cohen's kappa  $\kappa = 0.22$  and  $\kappa = 0.18$ , respectively. The raters reported the same score in 66% of cases.

### 3.2.3 | Advanced ioMRI quantification

Quantitative maps of dMRI data could be generated with sufficient SNR (absolute WM SNR two RF coils:  $21.9 \pm 13.8$ , four RF coils:  $19.4 \pm 14.0$ ). Averages of the dMRI metrics FA and MD did not differ statistically significantly between the setups with two and four RF coils in the CST and AF tracts. The standard deviations of these dMRI metrics decreased consistently, yet marginally, in the four RF coils setup. Similarly, quantified ASL CBF maps could be generated with sufficient SNR (absolute GM SNR two RF coils:  $3.17 \pm 2.07$ , four RF coils:  $2.49 \pm 1.42$ ). Mean quantified ASL CBF did also not differ statistically significantly between both setups in left (two RF coils:  $47.6 \pm 10.4$ , four RF coils:  $50.7 \pm 8.36 \text{ mL/100 g/min}$ ) or right GM (two RF coils:  $47.2 \pm 9.74$ , four RF coils:  $49.7 \pm 6.96 \text{ mL/100 g/min}$ ). The standard deviation of ASL CBF decreased in the four RF coils setup.

## 4 | DISCUSSION

In this study, we found that we could quantify ASL CBF in the surgical prone position and that these values did not differ from the supine position in any of the investigated ROIs or the whole brain. For this reason, we integrated the ASL sequence into our advanced pediatric ioMRI protocol. We found that SNR and CNR were higher in the setup with four RF coils. Moreover, all T1w, T2w, ASL, and dMR images were rated as clinically

acceptable or better and did not differ strongly between setups. A more substantial improvement in image quality of images acquired in the setup with four RF coils was seen for the nonweighted multishell dMRI maps that also yielded reduced susceptibility artifacts and the CST reconstructions. Quantified dMRI FA, MD, and ASL CBF were similar in both setups, but the standard deviations of these measures decreased in the setup with four RF coils.

To the best of our knowledge, the current study is the first to describe the effect of the surgical prone position on the quantification of ASL in the literature. Despite a difference in orientation and rotation of ASL-labeled arteries in the prone position, the measured ASL efficiency remained within the range of Chen et al.<sup>14</sup> This result supports the accuracy of our ASL CBF quantification.<sup>32</sup> Nevertheless, some lower-located brain regions showed slightly reduced ASL CBF in the prone position, which was potentially attributed to a weaker signal picked up in these regions by the 32-channel head coil due to the experimental prone position. This could have impacted the measurement accuracy. However, these discrepancies in ASL CBF between positions disappeared in the setup with two RF coils. Moreover, in this study we were unable to study the effect of anesthesia on the ASL CBF measurements.<sup>33</sup> However, this effect can be mitigated when performing preoperative and intraoperative ASL CBF measurements under the same anesthetics on the day of surgery. Consequently, we recommend comparing ASL CBF values obtained intraoperatively within the same patient, rather than between different patients.

Our developed advanced iMRI protocol with four RF coils did indeed yield higher SNR and CNR; this, however, was only marginally translated to improved image quality. Potentially, the difference between acceptable and better image quality was too subjective or small to be accurately determined by visual comparison. This might have indirectly introduced a bias that could have influenced the fair interobserver agreement. Alternatively, the increased SNR has reached a threshold, after which a further increase in SNR does not result in higher image quality. Nevertheless, both protocols were rated at least clinically acceptable, which confirmed our expectation of valid use of advanced MRI sequences in the surgical setting.<sup>11</sup> The increased number of RF coils did reduce artifacts in the images, which was best seen in the dMRI-derived images. These images showed fewer susceptibility artifacts with higher SENSE factors in the setup with four RF coils.<sup>16</sup> This impact on EPI images could be particularly beneficial in mitigating artifacts induced by fixation head pins used with the DORO surgical head fixation frame when scanning patients. Advanced iMRI metrics also benefited from the increased signal and SENSE factor as their metrics showed lower standard deviations.<sup>32,34</sup>

This study has some limitations. First, the mimicked prone position was less comfortable than the supine position for the subjects. This discomfort could have influenced the heart rate and blood pressure of subjects and, hence, the CBF measurements. However, we tried to mediate this with short scan protocols in each position and extra cushioning. Moreover, in the intraoperative setting, this limitation does not occur as the heads are fixated and the patient is anesthetized. Second, we were unable to evaluate the effects of the patient positioning and RF coils in our target population because of ethical considerations under Dutch law when scanning children. Nonetheless, we expect that the results in children would be similar to those observed in our included healthy adult study population. Third, the spatial overlap, for maximum decoupling, of the neighboring RF coils has been a priori determined, but in vivo, we cannot rule out that some variation in positioning has occurred. However, we assume that this variation has a negligible effect on the SNR and SENSE possibilities. Fourth, in theory, the SNR and *g*-factor would further increase with more than four RF coils.<sup>16,35</sup> However, in neurosurgical practice, this would not fit with the current DORO surgical head fixation frame that is used. Alternatively, the NORAS head-frame with eight integrated receive channels<sup>3</sup> could yield even higher SNR than our setup with four RF coils. However, the advantage of the DORO frame that we used in our setup is that it offers more surgical flexibility. Fifth, the generalizability of our findings could be affected by the small sample sizes; this is, however, mitigated by the use of paired statistical tests. The generalizability could also be affected by using two interface boxes to mimic an interface box with four sockets for RF coils that is not yet commercially available. Nevertheless, the generalizability will improve once this interface box with four sockets becomes available. Moreover, it is worth noting that single-channel RF coils are provided by all MR vendors.

In the future, we would like to analyze advanced MRI data of children who undergo brain tumor surgery to understand the effect of the mechanical manipulation on their brains.<sup>3-5</sup> Our validated ASL protocol in the prone position could be used for intraoperative CBF management to help identify brain regions at risk. This could guide neurosurgeons to make informed decisions during the procedure.<sup>6</sup> Our developed multishell dMRI protocol, which the neuroradiologists have approved, can be used to update the fiber tractography. Such an update could prevent surgery-associated neurological deficits.<sup>2,7-9</sup> Lastly, the four RF coils with additional SNR and increased SENSE factors could also reduce the scan time, instead of further improving image quality. Minimizing the MRI acquisition time of patients under anesthesia is important for their recovery after surgery.<sup>36</sup>

Taken together, this work has investigated practical use of advanced iMRI during pediatric neurosurgery. We concluded that ASL CBF quantification in the surgical prone position is valid. Moreover, ASL and multishell dMRI acquisition during surgery is possible with two RF coils. With just four RF coils, the SNR already increased over the typical two RF coils setup and these advanced MR sequences became less sensitive to artifacts.

## ACKNOWLEDGMENTS

We would like to thank Dennis W. J. Klomp for providing in-depth feedback on the paper, Jeroen C. W. Siero for his help with the development of the PCASL protocol with four RF coils, and J. Petr for his help with the ExploreASL analysis. We gratefully acknowledge funding of the European Union: Eurostars E! 12449 IMAGINE! and the Dutch Research Council: NWO-VIDI 18361\_JW.

## CONFLICT OF INTEREST STATEMENT

None of the authors have a conflict of interest to disclose.

## ORCID

Alberto De Luca  <https://orcid.org/0000-0002-2553-7299>

## REFERENCES

- Choudhri AF, Siddiqui A, Klimo P, Boop FA. Intraoperative MRI in pediatric brain tumors. *Pediatr Radiol*. 2015;45:397-405. doi:10.1007/s00247-015-3322-z
- Tejada S, Avula S, Pettorini B, Henningan D, Abernethy L, Mallucci C. The impact of intraoperative magnetic resonance in routine pediatric neurosurgical practice—a 6-year appraisal. *Childs Nerv Syst*. 2018;34:617-626. doi:10.1007/s00381-018-3751-8
- Abernethy LJ, Avula S, Hughes GM, Wright EJ, Mallucci CL. Intra-operative 3-T MRI for paediatric brain tumours: challenges and perspectives. *Pediatr Radiol*. 2012;42:147-157. doi:10.1007/s00247-011-2280-3
- Sanvito F, Castellano A, Falini A. Advancements in neuroimaging to unravel biological and molecular features of brain tumors. *Cancer*. 2021;13:424. doi:10.3390/cancers13030424
- Petr J, Hogeboom L, Nikulin P, et al. A systematic review on the use of quantitative imaging to detect cancer therapy adverse effects in normal-appearing brain tissue. *MAGMA*. 2022;35:163-186. doi:10.1007/s10334-021-00985-2
- Lindner T, Ahmeti H, Helle M, et al. Measurements of functional network connectivity using resting state arterial spin labeling during neurosurgery. *World Neurosurg*. 2022;157:152-158. doi:10.1016/j.wneu.2021.10.107
- Avula S, Kumar R, Pizer B, et al. Diffusion abnormalities on intraoperative magnetic resonance imaging as an early predictor for the risk of posterior fossa syndrome. *Neuro Oncol*. 2014;17:614-622. doi:10.1093/neuonc/nou299
- Giordano M, Samii A, Lawson McLean AC, et al. Intraoperative magnetic resonance imaging in pediatric neurosurgery: safety and utility. *J Neurosurg Pediatr*. 2017;19:77-84. doi:10.3171/2016.8.PEDS15708
- Low SYY, Soh SY, Chen MW, Ng LP, Low DCY, Seow WT. DTI fusion with conventional MR imaging in intra-operative MRI suite for paediatric brainstem glioma biopsy. *Childs Nerv Syst*. 2018;34:19-21. doi:10.1007/s00381-017-3627-3
- Saint-Martin C, Apuzzo S, Salman A, Farmer JP. Hyperacute infarct on intraoperative diffusion imaging of pediatric brain tumor surgery. *Can J Neurol Sci*. 2019;46:550-558. doi:10.1017/cjn.2019.226
- Jellema PEJ, Wijnen JP, De Luca A, et al. Advanced intraoperative MRI in pediatric brain tumor surgery. *Front Physiol*. 2023;14:1098959. doi:10.3389/fphys.2023.1098959
- Nejat F, El Khashab M, Rutka JT. Initial management of childhood brain tumors: neurosurgical considerations. *J Child Neurol*. 2008;23:1136-1148. doi:10.1177/0883073808321768
- Klein O, Boussard N, Guerbouz R, HELLERINGER M, Joud A, Puget S. Surgical approach to the posterior fossa in children, including anesthetic considerations and complications: the prone and the sitting position. Technical note. *Neurochirurgie*. 2021;67:46-51. doi:10.1016/j.neuchi.2020.04.128
- Chen Z, Zhang X, Yuan C, Zhao X, van Osch MJP. Measuring the labeling efficiency of pseudocontinuous arterial spin labeling. *Magn Reson Med*. 2017;77:1841-1852. doi:10.1002/mrm.26266
- Liu P, Parkinson C, Jiang D, et al. Characterization of MRI techniques to assess neonatal brain oxygenation and blood flow. *NMR Biomed*. 2019;32:e4103. doi:10.1002/nbm.4103
- Pruessmann KP. Parallel imaging at high field strength: synergies and joint potential. *Top Magn Reson Imaging*. 2004;15:237-244. doi:10.1097/01.mrm.0000139297.66742.4e
- Xie Y, Li Q. A review of deep learning methods for compressed sensing image reconstruction and its medical applications. *Electron*. 2022;11(4):586. doi:10.3390/electronics11040586
- Mutsaerts HJMM, Petr J, Thomas DL, et al. Comparison of arterial spin labeling registration strategies in the multi-center GENetic Frontotemporal dementia Initiative (GENFI). *J Magn Reson Imaging*. 2018;47:131-140. doi:10.1002/jmri.25751
- Mutsaerts HJMM, Petr J, Groot P, et al. ExploreASL: an image processing pipeline for multi-center ASL perfusion MRI studies. *Neuroimage*. 2020;219:117031. doi:10.1016/j.neuroimage.2020.117031
- Zhang Y, Brady M, Smith S. Segmentation of brain MR images through a hidden Markov random field model and the expectation-maximization algorithm. *IEEE Trans Med Imaging*. 2001;20:45-57. doi:10.1109/42.906424
- Wiens CN, Kisch SJ, Willig-Onwuachi JD, McKenzie CA. Computationally rapid method of estimating signal-to-noise ratio for phased array image reconstructions. *Magn Reson Med*. 2011;66:1192-1197. doi:10.1002/mrm.22893
- Guo F, Leemans A, Viergever MA, Dell'Acqua F, De Luca A. Generalized Richardson-Lucy (GRL) for analyzing multi-shell diffusion MRI data. *Neuroimage*. 2020;218:116948. doi:10.1016/j.neuroimage.2020.116948
- Leemans A, Jeurissen B, Sijbers J, Jones DK. ExploreDTI: a graphical toolbox for processing, analyzing, and visualizing diffusion MR data. *Proc Int Soc Magn Reson Med*. 2009;17:3537.
- Vos SB, Tax CMW, Luijten PR, Ourselin S, Leemans A, Froeling M. The importance of correcting for signal drift in diffusion MRI. *Magn Reson Med*. 2017;77:285-299. doi:10.1002/mrm.26124
- Leemans A, Jones DK. The B-matrix must be rotated when correcting for subject motion in DTI data. *Magn Reson Med*. 2009;61:1336-1349. doi:10.1002/mrm.21890
- Jensen JH, Helpert JA, Ramani A, Lu H, Kaczynski K. Diffusional kurtosis imaging: the quantification of non-Gaussian water diffusion by means of magnetic resonance imaging. *Magn Reson Med*. 2005;53:1432-1440. doi:10.1002/mrm.20508
- Zhang F, Ning L, O'Donnell LJ, Pasternak O. MK-Curve—characterizing the relation between mean kurtosis and alterations in the diffusion MRI signal fan. *Neuroimage*. 2019;196:68-80. doi:10.1016/j.neuroimage.2019.04.015
- Christiaanse E, Wyss PO, Scheel-Sailer A, et al. Mean kurtosis-Curve (MK-Curve) correction improves the test-retest reproducibility of diffusion kurtosis imaging at 3 T. *NMR Biomed*. 2023;36:e4856. doi:10.1002/nbm.4856

29. Zhang F, Wu Y, Norton I, et al. An anatomically curated fiber clustering white matter atlas for consistent white matter tract parcellation across the lifespan. *Neuroimage*. 2018;179:429-447. doi:[10.1016/j.neuroimage.2018.06.027](https://doi.org/10.1016/j.neuroimage.2018.06.027)
30. Jacobs SM, Versteeg E, van der Kolk AG, et al. Image quality and subject experience of quiet T1-weighted 7-T brain imaging using a silent gradient coil. *Eur Radiol Exp*. 2022;6(1):36. doi:[10.1186/s41747-022-00293-x](https://doi.org/10.1186/s41747-022-00293-x)
31. Fallatah SM, Pizzini FB, Gomez-Anson B, et al. A visual quality control scale for clinical arterial spin labeling images. *Eur Radiol Exp*. 2018;2(1):45. doi:[10.1186/s41747-018-0073-2](https://doi.org/10.1186/s41747-018-0073-2)
32. Alsop DC, Detre JA, Golay X, et al. Recommended implementation of ASL perfusion MRI for clinical applications. *Magn Reson Med*. 2015;73:102-116. doi:[10.1002/mrm.25197](https://doi.org/10.1002/mrm.25197)
33. Huhndorf M, Eimer C, Becher T, et al. Effect of general anesthesia on cerebral blood flow measured by arterial spin labeling: a retrospective study. *J Magn Reson Imaging*. 2022;58:663-665. doi:[10.1002/jmri.28507](https://doi.org/10.1002/jmri.28507)
34. Farrell JAD, Landman BA, Jones CK, et al. Effects of signal-to-noise ratio on the accuracy and reproducibility of diffusion tensor imaging-derived fractional anisotropy, mean diffusivity, and principal eigenvector measurements at 1.5T. *J Magn Reson Imaging*. 2007;26:756-767. doi:[10.1002/jmri.21053](https://doi.org/10.1002/jmri.21053)
35. Kim KN, Hernandez D, Seo JH, et al. Quantitative assessment of phased array coils with different numbers of receiving channels in terms of signal-to-noise ratio and spatial noise variation in magnetic resonance imaging. *PLoS ONE*. 2019;14(7):e0219407. doi:[10.1371/journal.pone.0219407](https://doi.org/10.1371/journal.pone.0219407)
36. Gandhe R, Bhave C. Intraoperative magnetic resonance imaging for neurosurgery—an anaesthesiologist's challenge. *Indian J Anaesth*. 2018;62:411-417. doi:[10.4103/ija.IJA\\_672\\_20](https://doi.org/10.4103/ija.IJA_672_20)

## SUPPORTING INFORMATION

Additional supporting information can be found online in the Supporting Information section at the end of this article.

**How to cite this article:** Jellema PEJ, Mannsdörfer LM, Visser F, et al. Improving advanced intraoperative MRI methods during pediatric neurosurgery. *NMR in Biomedicine*. 2024;37(6):e5124. doi:[10.1002/nbm.5124](https://doi.org/10.1002/nbm.5124)